

Viewpoint Paper

Characterization of thin films for solid oxide fuel cells facilitated by micropatterning

Thomas Ryll,* Jennifer L.M. Rupp, Anja Bieberle-Hutter,
Henning Galinski and Ludwig J. Gauckler

Nonmetallic Inorganic Materials, Department of Materials, ETH Zurich, Wolfgang-Pauli-Strasse 10, 8093 Zurich, Switzerland

Received 11 June 2010; accepted 13 September 2010

Available online 17 September 2010

Abstract—Micropatterning techniques offer the possibility of obtaining freely selectable thin film patterns with lateral dimensions down to the micrometer range. Furthermore, reaction sites can be systematically impacted or deactivated. This article reviews studies which have utilized these possibilities in order to characterize electrochemically electrode thin films for solid oxide fuel cells. In a second part, a processing route for the fabrication of characterization platforms, allowing for the electrical and electrochemical characterization of metal oxide thin films, is presented.

© 2010 Acta Materialia Inc. Published by Elsevier Ltd. All rights reserved.

Keywords: Fuel cell materials; Ceramic thin films; Electrical conductivity; Multilayers; Sputtering

1. Introduction

Within current research on planar solid oxide fuel cells (SOFCs), miniaturization and the reduction of operating temperatures are two lines of development [1–6]. Both objectives necessitate thin film components with thicknesses in the micrometer range. While thin films have gained significance in SOFC research, techniques for the micropatterning of thin films have become applicable for mechanistic studies as well as for the fabrication of thin film SOFC devices. In the silicon-based fabrication of microelectromechanical systems (MEMS) [7] techniques for micropatterning are well established. However, only some of these can be adopted for the micropatterning of oxidic SOFC electrode and electrolyte thin films. Others are not feasible or have to be modified, mainly due to the high temperatures required for the processing of oxidic thin films.

This article reviews how versatile microfabrication techniques have hitherto been used for the characterization of SOFC electrode thin films in literature. Following the overview, we discuss a detailed example and present a processing route for the fabrication of a characterization platform containing micropatterned $\text{La}_{0.56}\text{Sr}_{0.4}\text{Co}_{0.2}$ -

$\text{Fe}_{0.8}\text{O}_{3-\delta}$ (LSCF) cathode, $(\text{Y}_2\text{O}_3)_{0.08}(\text{ZrO}_2)_{0.92}$ (YSZ) electrolyte and Pt electrode thin films on a fused silica support. These devices aim at the comprehensive characterization of metal oxide thin films and their multilayers by DC and AC techniques.

2. Characterization of micropatterned SOFC electrode thin films

The key benefit of microfabrication techniques with respect to the characterization of SOFC thin films is the possibility to fabricate freely selectable thin film patterns with defined geometries and dimensions down to the micrometer range. The resulting control over the thin film surface area and its circumference, in case of SOFC electrode thin films referred to as the three-phase boundary (TPB), is used to gather insights into the electrochemical reaction pathways in SOFC components. The processes applied for the structuring of SOFC electrode thin films predominantly involve photolithographic structuring of photoresist and wet chemical etching as well as Ar^+ sputtering. Sintered electrolyte pellets or single crystals are mostly used as substrates. The following paragraphs overview the available literature ordered by the geometry of the applied thin film patterns.

Circular microelectrodes on SOFC electrolytes feature a simple geometry and well-defined relation between electrode area and TPB length [8]. Given a

* Corresponding author. Tel.: +41 44 632 71 56; fax: +41 44 632 11 32; e-mail: thomas.ryll@mat.ethz.ch

dense microstructure, they allow for a straightforward differentiation between microstructural- and material-related electrochemical effects. No reference electrode is required in the case of an extended counterelectrode and the ohmic resistance of the electrolyte is easily separated from the electrode impedance. As many microelectrodes can be fabricated and characterized in parallel on the same electrolyte sample, they are suitable for statistical studies. The low reaction area may prove a drawback in terms of a low impedance signal and the measurement of localized rather than averaged thin film properties. Furthermore, current constrictions are a source of error that potentially affects all micropatterned electrodes, and in the end requires finite-element modeling of electric fields for a proper interpretation of the data [9]. Accordingly, it needs to be taken into account that the operative reaction site might deviate from the geometrically accessible one due to the geometrically limited conductance of thin film patterns. Brichzin et al. [10,11] investigated the polarization resistance of dense $(\text{La}_{0.8}\text{Sr}_{0.2})_{0.92}\text{MnO}_{3-\delta}$ (LSM) microelectrodes as a function of diameter d and thickness t . A d^{-2} dependence with respect to the diameter and a linear correlation with the film thickness t were found. Hence, the bulk pathway is favored over the oxygen incorporation at the TPB, despite the poor oxygen conduction properties of LSM [12]. The same conclusion was drawn in studies presented by Hertz and Tuller [13] for microelectrodes of a Pt/yttria-stabilized zirconia (YSZ) composite and by Baumann et al. for $\text{La}_{0.6}\text{Sr}_{0.4}\text{Co}_{0.8}\text{Fe}_{0.2}\text{O}_{3-\delta}$ [14] and $\text{Ba}_{0.5}\text{Sr}_{0.5}\text{Co}_{0.8}\text{Fe}_{0.2}\text{O}_{3-\delta}$ [15] microelectrodes. In a continuation of this work, Baumann et al. found a strong enhancement of the electrode activity after replacing the A-side cation in $\text{La}_{1-x}\text{Sr}_x\text{Co}_{1-y}\text{Fe}_y\text{O}_{3-\delta}$ by Sm and Ba, again using circular microelectrodes [16].

Microelectrode arrays and interdigitated electrodes can be tailored to individual experimental approaches and provide the opportunity to achieve small and accurately adjustable distances between adjacent electrodes. These electrodes provide larger reaction areas than circular electrodes, and hence tend to produce an average performance. While microelectrode arrays, e.g. comb-shaped electrodes, are applied for cross-plane measurements using symmetrical cells or extended counterelectrodes, interdigitated electrodes allow for in-plane measurements on one side of the electrolyte. However, the geometrical complexity of interdigitated electrodes complicates the distribution of electrical fields and hence the interpretation of impedance data. Using comb-shaped electrode arrays on YSZ, a linear relationship between electrode conductance and TPB length was shown for Pt in air [17] and Ni in hydrogen atmospheres [18,19]. These studies confirmed that, in contrast to mixed-ionic–electronic conducting thin films, the rate-determining step on metallic Pt or Ni electrodes is confined to the close vicinity of the geometrical TPB. Furthermore, comb-shaped Ni electrode arrays on YSZ electrolytes characterized in hydrogen atmospheres have served as a model system for SOFC anodes in a number of studies [18–22]. The electrochemical performance of Ni anodes was shown to be subject to considerable relaxation and degradation processes [22]. Coarsening and agglomeration of the Ni thin film

patterns in hydrogen limited the measuring temperature to 700 °C and the minimum feature size to 5 μm [18,21].

Ar^+ sputtering as well as etching in dilute hydrochloric acid have been used for the micropatterning of mixed-ionic–electronic conducting $\text{La}_{0.6}\text{Sr}_{0.4}\text{Co}_{0.2}\text{Fe}_{0.8}\text{O}_{3-\delta}$ (LSCF) [23] and $\text{La}_{1-x}\text{Sr}_x\text{CoO}_3$ (LSC) thin films [24,25]. The latter study provided an indication that, in addition to the electrode material, interfacial reactions and the choice of substrate affect the feasibility of micropatterned SOFC thin films. Furthermore, interdigitated LSC patterns with stripe widths between 25 and 100 μm , investigated at temperatures below 400 °C, proved to be useful for the electrical characterization of the electrolyte. However, finer stripe widths below 25 μm and the use of reference electrodes were recommended by the authors in order to detect the electrode impedance in a reliable manner.

Finally, net-like electrode arrays of LSM on YSZ have been used by Horita et al. [26,27] in order to visualize the active sites for oxygen incorporation qualitatively by isotopic oxygen exchange experiments and adjacent secondary ion mass spectroscopy analysis.

Beyond the freely selectable patterning of thin film electrodes, microfabrication techniques provide the opportunity to manipulate electrode processes by selective deactivation of reaction sites. This possibility was first utilized by Brichzin et al. [11], who blocked the interface between circular LSM microelectrodes and the YSZ electrolyte by thin alumina discs. The increased electrode resistance emphasized the importance of the bulk path for the oxygen reduction reaction on thin LSM electrodes, in particular at high temperatures. A consistent conclusion was drawn by Koep et al. [28], who blocked the surface of patterned LSM electrodes with TiO_2 .

Studies investigating oxidic thin films for SOFCs commonly report a wide influence of processing conditions on the electrical and electrochemical properties. In addition to the investigation of these structure–property relations, it is increasingly important to characterize the electrochemical properties of thin film couples, multilayers and free-standing membranes. In this regard micropatterning techniques will make a contribution by facilitating the miniaturization of complete thin film SOFC devices [3] as well as the comprehensive characterization of SOFC thin films on miniaturized samples.

3. Example for a characterization platform for micropatterned functional thin films

The following fabrication route was used to fabricate characterization platforms featuring freely selectable but accurately defined thin film patterns suited for statistical studies. Results for the electrical in-plane conductivity of $\text{La}_{0.56}\text{Sr}_{0.4}\text{Co}_{0.2}\text{Fe}_{0.8}\text{O}_{3-\delta}$ (LSCF) thin film stripes and the cross-plane conductivity of $(\text{Y}_2\text{O}_3)_{0.08}(\text{ZrO}_2)_{0.92}$ (YSZ) thin films are shown by way of example and compared to literature data.

3.1. Experimental

Five hundred micrometers thick fused silica wafers (double side polished, University Wafer, USA) were used as substrates for the platform. Fused silica has been

preferred over silicon wafers in order to avoid parasitic impedances related to a conductive substrate as experienced in the literature [24,29]. The sample fabrication routine for micropatterned metal oxide thin films and their contacts is depicted in Figure 1A. On the right-hand side the stepwise buildup of multilayer structures designed for impedance measurements is shown. Detailed processing parameters for photolithography, sputtering of Pt and Ta, and deposition of LSCF and YSZ by pulsed laser deposition (PLD) are given in Tables 1–3, respectively. Masks printed on commercially available transparencies were applied during photolithography.

The sample fabrication route started with the photolithographic structuring of negative ma-N 1410 photoresist (micro resist, Germany) (Table 1). Adjacently a Ta|Pt double layer was deposited by sputtering (see Table 2 for detailed parameters). 10 nm of Ta were applied in order to promote the adhesion of the 100 nm thick Pt film. After stripping of the photoresist, micropatterned Ta|Pt electrodes, Pt contact paths and Pt contact pads remained on the substrate. Subsequently, a 100 nm thick LSCF thin film was deposited by PLD solely on the area designed for the multilayer specimen subjected to impedance measurements (Table 3). A mask of stainless steel prevented the rest of the substrate area from being coated during PLD. The LSCF film was micropatterned using photolithographic structuring of positive photoresist and Ar⁺ sputtering (Fig. 2A, inset), whereby LSCF thin film patterns with a feature size in

the range of 20–850 μm were obtained. The same area of the sample was coated by a 600 nm thick YSZ electrolyte thin film during the following fabrication step. Subsequently, a 100 nm thick LSCF thin film was deposited on the entire area for electrical and electrochemical characterization by PLD and likewise structured by Ar⁺ sputtering. The deposition and micropatterning of Pt top electrodes completed the sample fabrication.

The resulting micropatterns and thin film microstructures were examined by light microscopy (Eclipse L200D, Nikon, Japan) and scanning electron microscopy (Leo 1530, Carl Zeiss SMT, Germany). Cross-sections were cut, polished and imaged on a focused ion beam (FIB) workstation (NVISION 40, Carl Zeiss).

During electrical and electrochemical characterization, Ta|Pt contact pads were contacted by microprobes on a hot-plate. The measurement temperature was controlled in the range of 25–500 °C by a thermocouple touching the sample surface. A multimeter (Keithley 2700, Keithley, USA) and an impedance bridge (SI 1260, Solartron Analytical, UK) were used for DC conductivity and AC electrochemical impedance spectroscopy (EIS) measurements, respectively. EIS measurements were conducted in a two-point mode on the asymmetric air|Pt|LSCF|YSZ|LSCF|Pt|Ta|SiO₂ configuration. The excitation frequency during EIS ranged from 50 mHz to 10 MHz with an amplitude of 20 mV. At 350 °C the impedance spectra showed one high-frequency arc in the 50 kHz–10 MHz range and a clearly separated low-frequency feature between 0.01 and 10 Hz. The high-frequency arc was attributed to the electrolyte on the basis of the frequency range and its independence on an applied DC bias. Consequently, the low-frequency feature was ascribed to the electrodes.

3.2. Results and discussion

3.2.1. Micropatterning of LSCF thin films.

An overview image of the characterization platform fabricated in this study is shown in Figure 1B.

In order to pattern LSCF thin films on the platform Ar⁺ sputtering was used. The corresponding etching depth is plotted as a function of time in Figure 2A. The error bars are based on multiple thickness measurements on different areas of the sample. It was found that the etching depth depends linearly on time, resulting in an etching rate of 1.2 nm min⁻¹. This value is small compared to wet etching of LSCF in dilute hydrochloric acid, which usually yields etching rates of the order of hundreds of nanometers per minute [23]. However, the small etching rate allows for a precise control of the resulting film thicknesses. In addition, as Ar⁺ sputtering is a purely kinetic process, it is barely material dependent, and therefore transferable to other oxides. During etching, the positive AZ 1518 photoresist was removed at a rate of 8 nm min⁻¹ and etching times longer than 2 h resulted in burning of the photoresist and incomplete resist removal after the processing. Consequently, LSCF thin films to be patterned by Ar⁺ sputtering could not exceed 270 nm, given that the initial resist thickness was around 1.8 μm. A cross-sectional SEM image of a LSCF thin film edge after 110 min of Ar⁺ sputtering is shown in Figure 2B. It becomes apparent that the

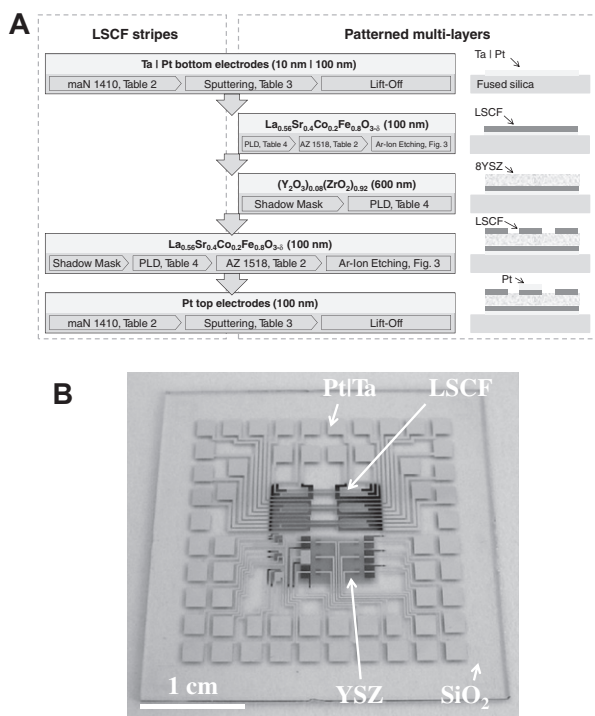


Figure 1. (A) Fabrication route for characterization platforms containing micropatterned La_{0.56}Sr_{0.4}Co_{0.2}Fe_{0.8}O_{3-δ} (LSCF), (Y₂O₃)_{0.08}(ZrO₂)_{0.92} (YSZ) and Pt|Ta thin films on amorphous silica. Photolithographic processes are denoted by the two applied photoresists ma-N 1410 and AZ 1518. Left: LSCF thin film stripes. Right: Micropatterned multilayers with the top-down layer sequence Pt|LSCF|YSZ|LSCF|Pt|Ta|SiO₂. (B) Overview image of a multilayer device containing micropatterned LSCF, YSZ and Pt|Ta thin films on amorphous silica.

Table 1. Processing parameters of photoresists applied for the photolithographic micropatterning of LSCF and Pt/Ta thin films.

	Structuring of Pt/Ta by lift-off	Structuring of LSCF by Ar plasma etching
Photoresists	ma-N 1410 (micro resist, Germany)	AZ 1518 (Clariant, Germany)
Dehydration	180 °C, 10 min	180 °C, 10 min
Adhesion promoter	Substrate exposed to the vapor of hexamethyldisilazane (Merck, Germany) in a closed glass jar, 60 °C, 10 min	–
Heat treatment	120 °C, 90 s	–
Spin coating	3000 rpm, 30 s	4000 rpm, 30 s
Pre-bake	120 °C, 90 s	100 °C, 50 s
Exposure	405 nm, 450 mJ cm ⁻²	405 nm, 450 mJ cm ⁻²
Development	ma-D533S (micro resist, Germany), 90 s	AZ 726MIF (Clariant, Germany), 90 s
Post-bake	–	115 °C, 50 s
Removal	Acetone, 5 min	Acetone, ultrasonic bath, 20 min

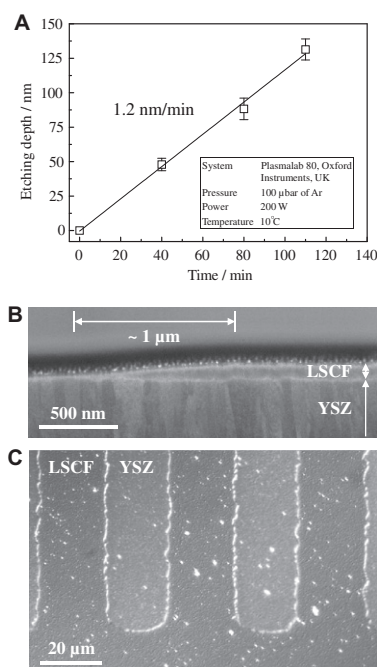
Table 2. Parameters used for the deposition of Pt and Ta thin films by sputtering.

	Ta	Pt
Sputter system	PVD products Inc., USA	
Target-substrate distance	160 mm	160 mm
Target-substrate tilt angle	35°	35°
Base pressure	10 ⁻⁹ bar	10 ⁻⁹ bar
Deposition pressure	4 × 10 ⁻⁶ bar of Ar	27 × 10 ⁻⁶ bar of Ar
Power	150 W	360 W
Temperature	No heating	No heating
Time	49 s	90 s
Deposition rate	0.20 nm s ⁻¹	1.14 nm s ⁻¹

Table 3. Parameters used for the deposition of LSCF and YSZ thin films by pulsed laser deposition.

	La _{0.56} Sr _{0.4} Co _{0.2} Fe _{0.8} O _{3-δ} (LSCF)	(Y ₂ O ₃) _{0.08} (ZrO ₂) _{0.92} (8YSZ)
Base pressure	4 × 10 ⁻⁹ bar	4 × 10 ⁻⁹ bar
Target-substrate distance	55 mm	85 mm
Deposition pressure	0.13 × 10 ⁻³ bar of O ₂	27 × 10 ⁻⁶ bar of O ₂
Temperature	600 °C	400 °C
Laser wavelength	248 nm	248 nm
Laser frequency	10 Hz	10 Hz
Fluence	2.44 J cm ⁻²	2.44 J cm ⁻²
Number of shots	3400	50,000
Deposition rate	0.29 nm s ⁻¹	0.06 nm s ⁻¹

etching edge is not vertical, but exhibits an approximately 1 μm wide ramp of reduced thickness, resulting in an edge angle of around 6°. This is due to the edge of the photoresist being removed from two sides during the Ar⁺ sputtering, which involves increasing flattening. However, in a study by Simrick et al. [23] similar etching conditions resulted in an edge angle of 75°. This difference might be due to the higher LSCF film thicknesses of 290 nm and potentially different ageing state of the photoresist. In Figure 2C, a top-view image of a comb-shaped LSCF pattern on a YSZ thin film taken by a light microscope is shown. Due to the application of a Nomarski filter in combination with polarized light, the pattern edges, as well as any asperities on the film surface, appear bright. The etching edges exhibit a lateral

**Figure 2.** (A) Etch depth plotted as a function of etching time for the Ar⁺ ion etching of LSCF thin films using the parameters specified in the inset. (B) Etching edge of a LSCF thin film after etching by Ar⁺ ions. The border area with decreasing film thickness is marked. (C) Top-view image of LSCF stripes on SiO₂ fabricated by Ar⁺ ion etching.

waviness of the order of 2 μm, which traces back to the wavy edges on the photolithography masks printed on transparencies. Nevertheless, this approach was chosen since it allows for a quick and cheap modification of the thin film patterns and does not impair the pattern quality as long as no perfectly smooth edges are required. In this case the use of Cr masks would improve the edge quality considerably. In contrast to reports for the wet etching of LSC thin films [25], no cracks or perforated border areas formed. The smallest width of LSCF stripes fabricated in this study was 20 μm. On the basis of the processing parameters presented in this study, pattern widths down to 5 μm are, however, feasible.

3.2.2. Electrical characterization of LSCF and YSZ thin films.

DC measurements of electrical in-plane

conductivity were performed on 100 nm thick LSCF thin film stripes with a line width and spacing of 300 μm , deposited by PLD and contacted by Pt contact paths. In Figure 3A, a schematic cross-section of the sample geometry is shown. A top-view image of a Pt contact path in contact with an LSCF stripe taken by light microscopy is available in Figure 3B. In Figure 3C, the in-plane conductivity of the LSCF thin film stripes is plotted as a function of temperature. The error bars account for the statistical error evaluated by several measurements on two characterization platforms. Patterned LSCF thin films deposited by PLD exhibited a thermally activated conductivity with a maximum value of $2.5 \times 10^3 \text{ S m}^{-1}$ at 500 $^\circ\text{C}$. The activation energy between 60 and 350 $^\circ\text{C}$ was 0.22 eV. For comparison, the conductivity of similarly patterned LSCF thin films deposited by spray pyrolysis [30] and literature data for LSCF thin films deposited by spray pyrolysis [31] and bulk LSCF [32] measured on macroscopic samples are given. Compared to the patterned LSCF thin film deposited by spray pyrolysis, the PLD films exhibited a 1.3 times higher conductivity at 500 $^\circ\text{C}$ but similar activation energy. The slightly lower conductivity results from the porosity of the sprayed film in the range of 10 vol.%. The in-plane conductivity of micropatterned LSCF thin films matches the literature data for LSCF thin films. Hence, no influence of micropatterning on the electrical conductivity of LSCF thin films is found. By contrast the in-plane conductivity of micropatterned LSCF thin films is around one order of magnitude lower than the corresponding bulk conductiv-

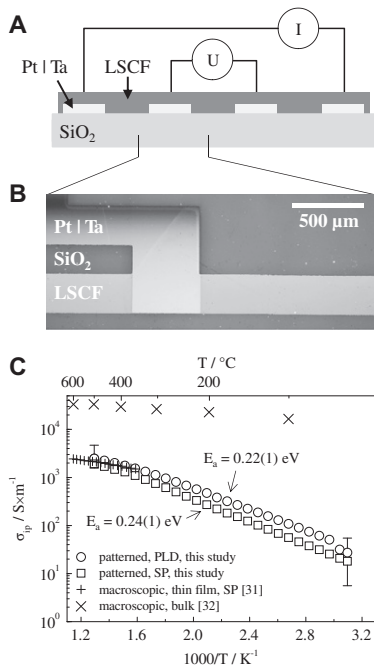


Figure 3. (A) Cross-sectional schematic of thin film patterns applied for the characterization of $\text{La}_{0.56}\text{Sr}_{0.4}\text{Co}_{0.2}\text{Fe}_{0.8}\text{O}_{3-\delta}$ (LSCF) thin films with respect to in-plane conductivity. (B) Light microscopic detail image of a LSCF thin film stripe contacted by a Pt|Ta contact path. (C) Electrical in-plane conductivity of LSCF thin film stripes deposited by pulsed laser deposition on an amorphous silica wafer. The activation energy in the temperature range between 60 and 350 $^\circ\text{C}$ and literature data for an LSCF thin film with the same composition deposited by spray pyrolysis [31] as well as bulk samples [32] are also shown.

ity. This difference is usually attributed to the much larger grain boundary area per unit volume in thin films due to the small grain sizes.

In addition to LSCF stripes, micropatterned multilayers exhibiting the top-down film sequence Pt|LSCF|YSZ|LSCF|Pt|Ta|SiO₂ were studied in order to characterize the YSZ electrolyte thin films with respect to their cross-plane conductivity. As the cross-plane conductivity of YSZ electrolyte thin films is a key factor for the performance of future thin film SOFCs, reliable techniques for its measurement are required. In order to separate the ionic conduction through the electrolyte from the polarization resistance of the electrodes and ohmic resistances arising from the Pt contacts, EIS was preferred over DC measurements. In Figure 4A, a schematic cross-section of the sample geometry is shown. An SEM image of a FIB-cut cross-section through the multilayer illustrates the microstructure—see Figure 4B. Although the sample was subjected to several heating cycles up to a maximum temperature of 420 $^\circ\text{C}$, no delamination or cracks were observed. While the oxidic LSCF and YSZ thin films are dense, some voids can be seen at the grain boundaries of the Pt contact films. The high-frequency arc in the impedance spectra measured across the multilayers was attributed to the electrolyte thin film. In Figure 4C, the corresponding cross-plane conductivity of the 600 nm thick YSZ electrolyte thin films deposited by PLD is plotted as a function of temperature. At 400 $^\circ\text{C}$ the YSZ film exhibited a cross-plane conductivity of $6 \times 10^{-3} \text{ S m}^{-1}$, while an activation energy of 0.9(1) eV was measured between 200 and 450 $^\circ\text{C}$. The activation energy as well as the conductivity correspond to the literature data for the cross-plane and in-plane conductivity of YSZ thin films

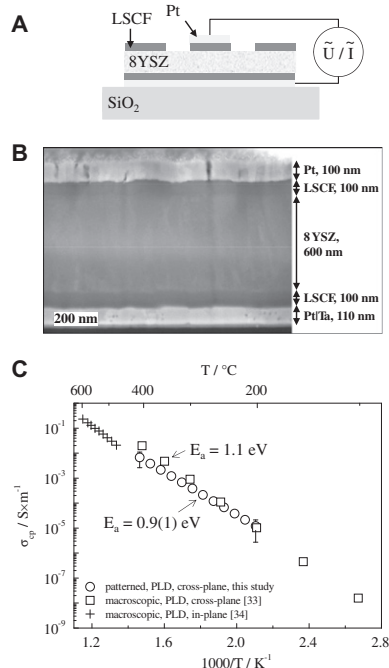


Figure 4. (A) Cross-sectional schematic of thin film patterns used for the characterization of $(\text{Y}_2\text{O}_3)_{0.08}(\text{ZrO}_2)_{0.92}$ (YSZ) electrolyte thin films with respect to cross-plane conductivity. (B) FIB-polished cross-section of a patterned multilayer Pt|LSCF|YSZ|LSCF|Pt|Ta|SiO₂. (C) Cross-plane conductivity of a YSZ electrolyte thin film plotted as a function of temperature. Literature data is also given [33,34].

deposited by PLD and measured on macroscopic samples [33,34]. This finding confirms (i) that micropatterning does not impact the cross-plane conductivity of YSZ thin films deposited by PLD and (ii) that patterned multilayers can be used to characterize oxidic electrolyte thin films with respect to their cross-plane conductivity.

4. Conclusions

A literature review showed that micropatterning techniques offer versatile possibilities for the characterization of SOFC electrode thin films with respect to thin film properties and the identification of reaction mechanisms. As the literature data in this context is scarce with respect to processing parameters, we identified a processing route for the fabrication of characterization platforms comprising Pt|Ta, LSCF and YSZ thin films on amorphous SiO₂ wafers. Detailed processing parameters for the thin film deposition by sputtering and PLD as well as for micropatterning using photolithography techniques and Ar⁺ sputtering were specified. Such platforms facilitate a comprehensive and statistically significant characterization of oxidic thin films on a comparable basis.

Micropatterned LSCF stripes are reported to show an electrical in-plane conductivity comparable to unmicropatterned thin films. Hence, the proposed structuring route based on photolithography and Ar⁺ sputtering does not alter the electrical properties of LSCF thin films.

Multilayer structures exhibiting the top-down sequence Pt|LSCF|YSZ|LSCF|Pt|Ta|SiO₂ were successfully deposited and micropatterned with feature sizes down to 20 μm. Cross-plane impedance measurements were clearly separated into electrolyte and electrode contributions. The cross-plane conductivity of the YSZ electrolyte thin films embedded in this multilayer structure agrees with the in- and cross-plane conductivity of single thin films.

Future studies will focus on the electrochemical characterization of micropatterned LSCF thin films on thin film electrolytes. Both the ability to fabricate patterned electrode–electrolyte multilayers as well as the electrical and electrochemical characterization of thin film electrodes in contact with electrolyte thin films are prerequisites for the development of thin film SOFCs.

Acknowledgements

The authors would like to thank the FIRST Center for Micro- and Nanoscience and the Electron Microscopy Center (EMEZ) at ETH Zurich for support. Financial assistance by the following Swiss institutions is gratefully acknowledged: (i) Competence Center for Materials Science and Technology (CCMX) within the framework of the NANCER project; (ii) Center of Competence Energy and Mobility (CEEM) within the framework of the ONEBAT project; (iii) Swiss Electric Research (SER) within the framework of the ONEBAT project; (iv) Swiss National Foundation (SNF) within the framework of the Sinergia project ONEBAT.

References

- [1] D. Beckel, A. Bieberle-Hutter, A. Harvey, A. Infortuna, U.P. Muecke, M. Prestat, J.L.M. Rupp, L.J. Gauckler, *J. Power Sources* 173 (2007) 325.
- [2] D. Nikbin, *Fuel Cell Rev.* 3 (2006) 21.
- [3] A. Evans, A. Bieberle-Hütter, J.L.M. Rupp, L.J. Gauckler, *J. Power Sources* 194 (2009) 119.
- [4] B.C.H. Steele, A. Heinzel, *Nature* 414 (2001) 345.
- [5] A. Weber, E. Ivers-Tiffée, in: *Eighth Ulm Electro-Chemical Talks on Electrochemical Energy Conversion and Storage*, 2002, p. 273.
- [6] J. Will, A. Mitterdorfer, C. Kleinlogel, D. Perednis, L.J. Gauckler, *Solid State Ionics* 131 (2000) 79.
- [7] K.D. Wise, *Sens. Actuators A* 136 (2007) 39.
- [8] J. Fleig, F.S. Baumann, V. Brichzin, H.R. Kim, J. Jamnik, G. Cristiani, H.U. Habermeier, J. Maier, *Fuel Cells* 6 (2006) 284.
- [9] J.L. Hertz, H.L. Tuller, *Solid State Ionics* 178 (2007) 915.
- [10] V. Brichzin, J. Fleig, H.U. Habermeier, J. Maier, *Electrochem. Solid State* 3 (2000) 403.
- [11] V. Brichzin, J. Fleig, H.U. Habermeier, G. Cristiani, J. Maier, *Solid State Ionics* 152 (2002) 499.
- [12] R.A. De Souza, J.A. Kilner, J.F. Walker, *Mater. Lett.* 43 (2000) 43.
- [13] J.L. Hertz, H.L. Tuller, *J. Electrochem. Soc.* 154 (2007) B413.
- [14] F.S. Baumann, J. Fleig, H.U. Habermeier, J. Maier, *Solid State Ionics* 177 (2006) 1071.
- [15] F.S. Baumann, J. Fleig, H.U. Habermeier, J. Maier, *Solid State Ionics* 177 (2006) 3187.
- [16] F.S. Baumann, J. Fleig, G. Cristiani, B. Stuhlhofer, H.U. Habermeier, J. Maier, *J. Electrochem. Soc.* 154 (2007) B931.
- [17] R. Radhakrishnan, A.V. Virkar, S.C. Singhal, *J. Electrochem. Soc.* 152 (2005) A927.
- [18] J. Mizusaki, H. Tagawa, T. Saito, K. Kamitani, T. Yamamura, K. Hirano, S. Ehara, T. Takagi, T. Hikita, M. Ippommatsu, S. Nakagawa, K. Hashimoto, *J. Electrochem. Soc.* 141 (1994) 2129.
- [19] A. Bieberle, L.P. Meier, L.J. Gauckler, *J. Electrochem. Soc.* 148 (2001) A646.
- [20] A. Bieberle, L.J. Gauckler, *Solid State Ionics* 135 (2000) 337.
- [21] A.M. Sukeshini, B. Habibzadeh, B.P. Becker, C.A. Stoltz, B.W. Eichhorn, G.S. Jackson, *J. Electrochem. Soc.* 153 (2006) A705.
- [22] A. Utz, H. Stormer, A. Leonide, A. Weber, E. Ivers-Tiffée, *J. Electrochem. Soc.* 157 (2010) B920.
- [23] N.J. Simrick, et al., *Solid State Ionics* (2010), doi:10.1016/j.ssi.2010.03.025.
- [24] A. Bieberle-Hutter, M. Sogaard, H.L. Tuller, *Solid State Ionics* 177 (2006) 1969.
- [25] A. Bieberle-Hutter, H.L. Tuller, *J. Electroceram.* 16 (2006) 151.
- [26] T. Horita, K. Yamaji, M. Ishikawa, N. Sakai, H. Yokokawa, T. Kawada, T. Kato, *J. Electrochem. Soc.* 145 (1998) 3196.
- [27] T. Horita, K. Yamaji, N. Sakai, H. Yokokawa, T. Kato, *J. Electrochem. Soc.* 148 (2001) J25.
- [28] E. Koep, C. Compson, M. Liu, Z. Zhou, *Solid State Ionics* 176 (2005) 1.
- [29] A.C. Johnson, B.K. Lai, H. Xiong, S. Ramanathan, *J. Power Sources* 186 (2009) 252.
- [30] D. Beckel, A. Dubach, A.R. Studart, L.J. Gauckler, *J. Electroceram.* 16 (2006) 221.
- [31] D. Beckel, A. Dubach, A.N. Grundy, A. Infortuna, L.J. Gauckler, *J. Eur. Ceram. Soc.* 28 (2008) 49.
- [32] L.W. Tai, M.M. Nasrallah, H.U. Anderson, D.M. Sparlin, S.R. Sehlin, *Solid State Ionics* 76 (1995) 273.
- [33] U.P. Muecke, D. Beckel, A. Bernard, A. Bieberle-Hutter, S. Graf, A. Infortuna, P. Muller, J.L.M. Rupp, J. Schneider, L.J. Gauckler, *Adv. Funct. Mater.* 18 (2008) 3158.
- [34] S. Heiroth, T. Lippert, A. Wokaun, M. Dobeli, *Appl. Phys. A* 93 (2008) 639.